Probing the structure of a rotaxane with two-dimensional infrared spectroscopy

Olaf F. A. Larsen[†], Pavol Bodis[†‡], Wybren Jan Buma[‡§], Jeffrey S. Hannam[¶], David A. Leigh[§¶], and Sander Woutersen[†§]

[†]FOM Institute for Atomic and Molecular Physics, Kruislaan 407, 1098 SJ, Amsterdam, The Netherlands; [‡]Van 't Hoff Institute for Molecular Sciences, University of Amsterdam, Nieuwe Achtergracht 127-129, 1018 WV, Amsterdam, The Netherlands; and [¶]School of Chemistry, University of Edinburgh, The King's Buildings, West Mains Road, EH9 3JJ Edinburgh, United Kingdom

Edited by F. Fleming Crim, University of Wisconsin, Madison, WI, and approved August 4, 2005 (received for review June 24, 2005)

Femtosecond 2D-IR spectroscopy has been used to study the structure of a [2]rotaxane composed of a benzylic amide macrocycle that is mechanically interlocked onto a succinamide-based thread. Both the macrocycle and the thread contain carbonyl groups, and by determining the coupling between the stretching modes of these groups from the cross-peaks in the 2D-IR spectrum, the structure of the macrocycle–thread system has been probed. Our results demonstrate that 2D-IR spectroscopy can be used to observe structural changes in molecular devices on a picosecond time scale.

femtosecond IR spectroscopy | molecular machines

It has recently become possible to synthesize molecules that function like mechanical devices (1–4), such as switches (5–7), motors (8–11), brakes (12), turnstiles (13), and elevators (14). These manmade molecular machines can be considered as nanoscale versions of their macroscopic analogues. However, many well known macroscopic concepts no longer apply at a molecular level. For instance, the concept of viscous friction becomes meaningless as the size of moving object approaches that of the molecules of the surrounding medium and as the time scale of the motion approaches that of the molecules of this medium (15). This regime of device operation is a new one, where the elementary component motions (rotations around covalent bonds and the making and breaking of hydrogen bonds) and the fluctuations of the surroundings both take place on the picosecond or subpicosecond time scale. Hence, for a detailed understanding of the physics and chemistry of molecular devices, experiments that probe their motion on an ultrafast time scale are essential, and the insights obtained from such experiments should be important for potential applications.

A promising technique for such experiments is 2D-IR spectroscopy. With 2D-IR spectroscopy, molecular conformations are determined by measuring couplings between molecular vibrations. The method was inspired by multidimensional NMR spectroscopy, in which couplings between nuclear spins are used for structure resolution (16). Like nuclear spins, normal modes are often well localized in the molecule (especially when they involve stretching of specific chemical bonds), and the coupling between them is mainly dipolar. The 2D-IR spectrum can therefore give direct access to the conformation of a molecule or its parts (17–23). The important advantage of 2D-IR spectroscopy as compared with 2D-NMR spectroscopy is its time resolution: The conformation can be determined with a time resolution determined by the free-induction decay of the transition, which is generally <1 ps. As a consequence, 2D-IR spectroscopy can be used to study motion in molecular systems on a time scale comparable to that of the elementary molecular motions. To this purpose, one triggers the motion (typically with a short optical pulse) and monitors the subsequent structural changes by recording 2D-IR spectra at different time delays with respect to the external trigger. In this way, a "movie" of the molecular motion can be constructed (24). This experimental scheme has recently been realized to study optically triggered α-helix formation in a peptide with time-resolved 2D-IR spectroscopy (25) and to study thermally induced unfolding of a protein with dispersed vibrational echo spectroscopy (26). Applying such methods to study the motion of molecular devices, which, in many cases, can also be externally triggered (5, 27), will reveal fundamental aspects of their physics and chemistry.

Prototypical synthetic mechanical molecular devices are often based on mechanically interlocked architectures (rotaxanes and catenanes) to reduce the relative degrees of freedom of the components. We have therefore investigated whether the coconformation[‖] (28) of a rotaxane (1, 29) can be determined from its 2D-IR spectrum. We have chosen the [2]rotaxane shown in Fig. 1, which is composed of a benzylic amide macrocycle that is mechanically interlocked onto a succinamide-based thread and held in position by a network of hydrogen bonds (6). This rotaxane is representative of a large class of rotaxane- and catenane-based devices that includes molecular shuttles (5) and motors (10, 11). We will show that the 2D-IR spectrum can be used to determine the coconformation of the rotaxane: in particular, the distance and angle between the macrocycle and thread carbonyl groups (see Fig. 1). The time resolution of the structural probing is 1 ps.

Materials and Methods

Using the experimental setup described in ref. 30, we obtain mid-IR pulses with a duration of $\approx$150 fs at 1,650 cm^{-1} and an energy and bandwidth of 1 μJ and 200 cm^{-1}, respectively. A small fraction of the mid-IR pulses is split off to obtain broadband probe pulses. The remainder is passed through an IR Fabry–Perot filter, resulting in pump pulses with a bandwidth of 10 cm^{-1}, the center frequency of which is varied by adjusting the Fabry–Perot filter by using piezo-electric controllers. The pump pulses have an intensity envelope that is approximately single-sided exponential with a full width at half maximum of 500 fs, as determined from a cross-correlation measured by using two-photon absorption in InAs placed in a sample cell identical to the one used in the rotaxane experiment. Transient absorption changes are measured by frequency-dispersed detection of the probe and reference pulses. The [2]rotaxane was synthesized by following the procedure described in ref. 6. The experiments are carried out at room temperature on 2.5 mM solutions of the rotaxane in $CHCl_3$ kept between two CaF_2 windows separated by a 1-mm Teflon spacer.

Results and Discussion

1D and 2D Vibrational Spectrum. Fig. 2*a* shows the conventional IR absorption spectrum of the rotaxane in $CHCl_3$. The peaks at

This paper was submitted directly (Track II) to the PNAS office.

Freely available online through the PNAS open access option.

[§]To whom correspondence may be addressed. E-mail: wybren@science.uva.nl, david.leigh@ed.ac.uk, or s.woutersen@amolf.nl.

[‖]The term coconformation refers to the relative positions of noncovalently bonded or mechanically interlocked components with respect to each other.

www.pnas.org/cgi/doi/10.1073/pnas.0505313102

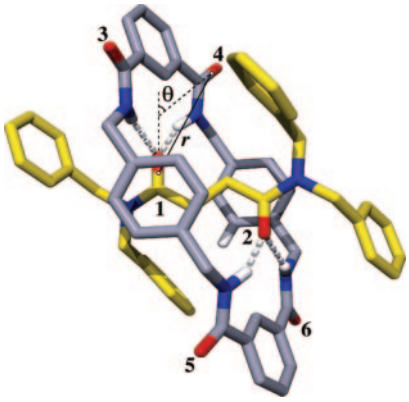

Fig. 1. X-ray crystal structure of the rotaxane that was investigated in this study (6). For clarity, the carbon atoms in the thread are colored yellow, and only hydrogen atoms that are involved in hydrogen bonds are shown. The carbonyl groups are numbered, and the distance r and angle θ that have been determined from the 2D-IR spectrum are indicated.

1,610 cm^{-1} and 1,660 cm^{-1} are due to the C═O-stretching modes of the thread (labeled 1 and 2 in Fig. 1) and the macrocycle (labeled 3–6), respectively, where the assignment of the peaks follows from comparing the spectrum of the rotaxane with that of the thread alone. Because of the symmetry of the rotaxane, the four C═O groups in the macrocycle are equivalent, and the same holds for the two C═O groups in the thread.

Fig. 2 *b* and *c* shows the 2D vibrational spectra of the rotaxane for parallel and perpendicular polarizations of the pump and probe pulses, respectively. At the diagonal of the graph, two intense positive–negative doublets are observed that arise from resonant excitation of the C═O-stretching modes of the macrocycle and the thread. Transfer of population from the $\nu = 0$ to the $\nu = 1$ state upon resonant excitation leads to a negative absorption change at the $\nu = 0 \rightarrow 1$ transition frequency (caused by bleaching and $\nu = 1 \rightarrow 0$ stimulated emission) and a positive absorption change at the $\nu = 1 \rightarrow 2$ transition frequency. Because the anharmonic shift Δ (the red-shift of the $\nu = 1 \rightarrow 2$ frequency with respect to the $\nu = 0 \rightarrow 1$ frequency) is comparable to the homogeneous line widths of the C═O-stretching modes, the positive and negative absorption changes overlap. Therefore, the negative extrema along the probe axis occur at frequencies slightly higher than the $\nu = 0 \rightarrow 1$ transition frequencies.

Macrocycle–Thread Coupling. In the off-diagonal (lower right and upper left) regions of the 2D spectrum, cross-peaks are observed, the most prominent of which are indicated by arrows in Fig. 2. The presence of these cross-peaks shows that the C═O-stretching modes of the macrocycle and the thread are coupled. Like the diagonal peaks, each cross-peak consists of a positive–negative doublet, which can be understood as follows. When there is a coupling between two modes a and b, the frequency of the state in which both modes are in the $\nu = 1$ state is $< \nu_a + \nu_b$ by the cross-anharmonicity x_{ab} (17). As a consequence, exciting one of the modes effectively gives rise to a change of $-x_{ab}$ in the frequency of the other. This frequency change is, in general, smaller than the line width, so the difference in absorption between the original and the shifted peak looks approximately like the derivative of the absorption band, and the height of the cross-peak is proportional to the coupling between the modes (17). For the cross-peak at the lower right in Fig. 2*c*, the positive–negative feature is clearly observed. The cross-peak in the upper left of the 2D plot overlaps with the much stronger $\nu = 1 \rightarrow 2$ excited-state absorption of the macrocycle C═O-stretching mode on the

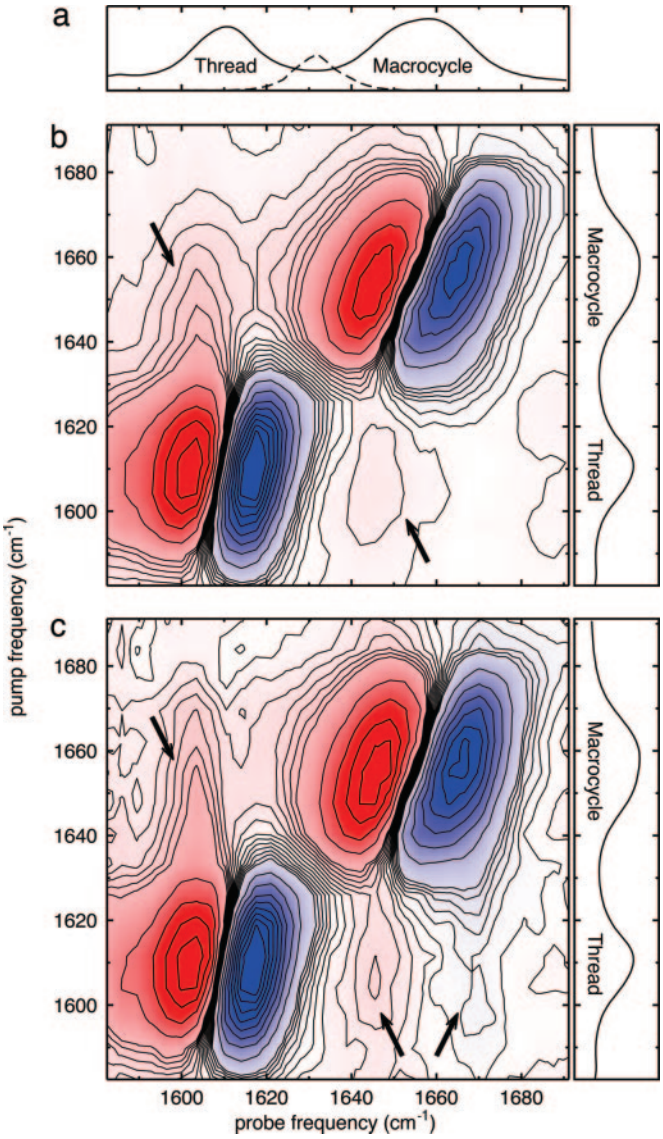

Fig. 2. Linear and 2D-IR spectra of the rotaxane shown in Fig. 1. (*a*) C═O-stretching region of the absorption spectrum of the rotaxane dissolved in $CHCl_3$ (solvent background is subtracted). Dashed line is the typical power spectrum of a pump pulse. (*b*) 2D spectrum of the rotaxane at a pump-probe delay of 1 ps for parallel polarizations of the pump and probe pulses, showing the transient absorption change $\Delta\alpha$ as a function of the pump and probe frequencies. Red indicates positive $\Delta\alpha$; blue indicates negative $\Delta\alpha$. The contour level spacing is 0.51 mOD. Five additional contours above and below $\Delta\alpha = 0$ are drawn with a level spacing of 0.085 mOD. (*c*) The same as in *b* but for perpendicular polarizations of the pump and probe pulses. The contour level spacing is 0.19 mOD. Five additional contours above and below $\Delta\alpha = 0$ are drawn with a level spacing of 0.032 mOD. The arrows indicate the most prominent cross-peaks.

diagonal, and the negative part of the cross-peak around $(\nu_{probe}, \nu_{pump}) = (1{,}620, 1{,}660)$ cm^{-1} is superimposed on the much bigger positive contribution from the diagonal peak. Fig. 3 shows horizontal cross sections at $\nu_{pump} = 1{,}610$ cm^{-1} through the 2D-IR spectra for parallel and perpendicular polarizations of the pump and probe pulses. The polarization dependence of the cross-peaks is clearly different from that of the peaks on the diagonal, which shows that the cross-peaks do not arise from excitation by the wing of the power spectrum of the pump. From the ratio of the parallel and perpendicular signals, we find that the anisotropy of the diagonal peak is 0.37,

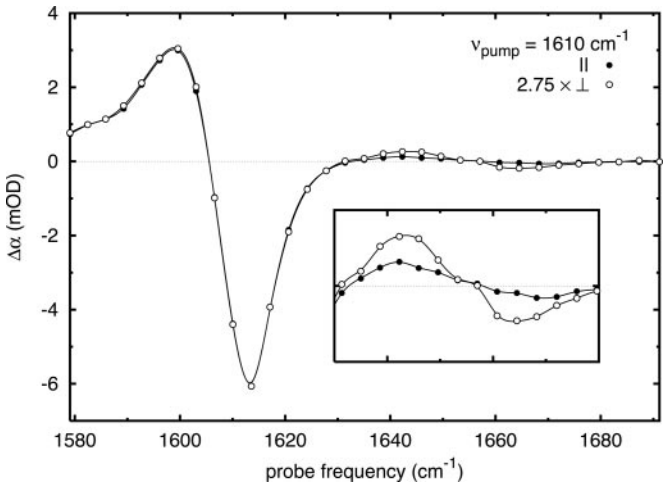

Fig. 3. Cross sections through the 2D spectra at ν_{pump} = 1,610 cm^{-1}. The spectrum for perpendicular pump and probe polarizations has been scaled to make the peaks at the diagonal equally large.

close to the theoretically expected value of 0.4 (31). The anisotropy of the cross-peak can be determined in the same way from the cross-peak amplitudes for parallel and perpendicular polarizations of pump and probe,[††] and we find a value of −0.05. Because of the localized nature of the eigenstates, the angle θ between the macrocycle and the thread carbonyl groups (see Fig. 1) can be directly derived from the cross-peak anisotropy (see "Semiquantitative Analysis" in the section that follows).

Structural Inhomogeneity. From the shape of the diagonal peaks, it is clearly seen that the spectral response of the thread and macrocycle C═O-stretching bands depends on the pump frequency: For low pump frequency, the positive and negative extrema occur at lower probing frequencies than for high pump frequency. This observation implies that the C═O-stretching bands are inhomogeneously broadened: There exists a distribution of C═O-stretching frequencies that is static on the time scale of the experiment. From the shape of the diagonal peaks, the homogeneous line width and the width of the spectral distribution can be determined (32–35), and we find that for both the macrocycle and the thread, the width of this distribution is larger than the couplings between the C═O-stretching modes (see *Quantitative Analysis*). The stretching frequency of a C═O group involved in a hydrogen bond depends on the length of this hydrogen bond (35, 36), and the spectral inhomogeneity of the C═O bands therefore most likely arises from a distribution of C═O···H hydrogen-bond lengths. Such distributions of C═O···H hydrogen-bond lengths have been observed previously in other molecular systems (37–40).

Quantitative Analysis

Model. To obtain estimates for the macrocycle–thread coupling and the widths of the inhomogeneous distributions of the macrocycle and thread frequencies, we have performed a least-squares fit of a calculated 2D spectrum to the experimental data. The cross-peak intensity is determined mainly by the magnitude of the coupling between neighboring C═O groups (the pairs 1–3, 1–4, 2–5, and 2–6 in Fig. 1). Because the coupling strength decreases rapidly with the distance between the coupled oscillators (41), the other macrocycle–thread couplings (e.g., in pair 1–6) are much smaller and contribute negligibly to the macrocycle–thread cross-peak intensity. The couplings between C═O groups within the macrocycle (e.g., pair 3–4) and between the C═O group modes within the thread (pair 1–2) might in principle lead to splittings of the macrocycle and thread absorption bands. However, because these couplings are small compared with the homogeneous line widths and the widths of the inhomogeneous distributions (see below), their magnitudes have a small influence on the 2D spectrum and hence cannot be determined from our experimental results. For this reason, we treat only the macrocycle–thread coupling β as a free parameter in the least-squares fit and keep all other couplings (macrocycle–macrocycle, thread–thread, and couplings between macrocycle and thread groups on opposing sides of the rotaxane) fixed at values that we obtain from density-functional calculations at the B3LYP/6-31G* level on the harmonic force fields of the isolated macrocycle and thread. From these calculations, we obtain the frequencies of the normal modes of the macrocycle and of the thread. There are four normal modes involving the C═O-stretching motions in the macrocycle, and from the differences between their frequencies, the couplings can be obtained. The same holds for the two C═O-stretching modes of the thread. Using the uncoupled C═O-stretching modes as the basis set and the numbering in Fig. 1, we obtain the following one-exciton Hamiltonian

$$H^{(1)} = \left(\begin{array}{cc|cccc} \varepsilon_1 & 2.7 & \beta & \beta & & \\ 2.7 & \varepsilon_2 & & & \beta & \beta \\ \hline \beta & & \varepsilon_3 & 2.7 & 0.2 & 0.1 \\ \beta & & 2.7 & \varepsilon_4 & 0.1 & 0.2 \\ & \beta & 0.2 & 0.1 & \varepsilon_5 & 2.7 \\ & \beta & 0.1 & 0.2 & 2.7 & \varepsilon_6 \end{array}\right), \qquad [1]$$

where the thread and macrocycle parts of the Hamiltonian have been separated by lines and the couplings have been expressed in cm^{-1}. The two-exciton Hamiltonian can be constructed from the one-exciton Hamiltonian in a straightforward way (42, 43), with the only additional parameters needed being the anharmonic shifts Δ_T and Δ_M (the difference between the $0 \rightarrow 1$ and $1 \rightarrow 2$ frequencies) of the thread and macrocycle C═O-stretching modes.

The eigenstates are obtained by diagonalizing the one- and two-exciton Hamiltonians, and the transition-dipole moments can be constructed from the localized transition dipoles by using the eigenvector coefficients. The directions of the transition-dipole vectors are obtained from the x-ray structure. We keep the direction of the transition dipoles in the macrocycle and in the thread fixed with respect to the macrocycle and the thread, respectively, but treat the angle θ between proximate macrocycle and thread dipoles (and hence, effectively, the orientation of the macrocycle relative to the thread) as a free parameter. In case of a distribution of angles, θ would represent an average of this distribution. From the eigenstates and transition dipoles, the 2D pump-probe response can be calculated (31, 42).

The line-broadening is taken into account by using the Bloch model (31, 44). For a particular molecular conformer, each transition has a homogeneous line width $2\Gamma_M$ or $2\Gamma_T$, which can be different for the macrocycle and thread C═O-stretching modes.[‡‡] The spectral inhomogeneity is modeled by independent Gaussian probability distributions for the site frequencies of the macrocycle and thread C═O groups (44):

[††]To eliminate the small background contribution of the diagonal peak at the position of the cross-peak, we use the difference between the positive maximum and negative minimum values as the amplitude.

[‡‡]The homogeneous dephasing rates of the $1 \rightarrow 2$ transitions are larger than those of the $0 \rightarrow 1$ transitions because the T_1 values of the $2 \rightarrow 1$ transitions are shorter than those of the $1 \rightarrow 0$ transition. We use the harmonic approximation (51) in which $T_1(2 \rightarrow 1) = \frac{1}{2}T_1(1 \rightarrow 0)$.

Table 1. Values of spectral parameters of the thread and macrocycle C=O-stretching modes obtained from the least-squares fit shown in Fig. 4

Parameter	Thread	Thread–macrocycle	Macrocycle
Δ, cm^{-1}	12 ± 3		9 ± 3
2Γ, cm^{-1}	10 ± 1		10 ± 1
σ, cm^{-1}	6.3 ± 0.5		7.9 ± 0.7
θ		48° ± 10°	
β, cm^{-1}		−3.3 ± 0.7	

$$P(\varepsilon_1, \ldots, \varepsilon_6) = \prod_{i=1,2} \frac{e^{-(\varepsilon_i - \bar{\varepsilon}_T)^2/2\sigma_T^2}}{\sqrt{2\pi\sigma_T}} \prod_{j\,=\,3\ldots6} \frac{e^{-(\varepsilon_j - \bar{\varepsilon}_M)^2/2\sigma_M^2}}{\sqrt{2\pi\sigma_M}}. \quad [2]$$

A homogeneous 2D spectrum can be calculated for each realization $\{\varepsilon_1, \varepsilon_2, \ldots, \varepsilon_6\}$, and by integration over all realizations, weighting with the above probability distribution, the ensemble-averaged 2D spectrum is obtained. This multidimensional integration is carried out numerically by using a Monte Carlo method (45). The parameters obtained from the least-squares fit are listed in Table 1, and the result of the fit is shown in Fig. 4.

Structural Parameters. From the fit, the angle θ (see Fig. 1) is found to be 48 ± 10°, which is comparable to the angle in the crystal structure. In the x-ray structure, the angles between the thread transition dipole and the transition dipoles of the two hydrogen-bonded macrocycle C=O groups are slightly different (50° and 68°); the average value is 59°. The small difference between the latter value and the θ found here suggests that the coconformations in solution and in the crystalline phase differ slightly, which may be due to packing effects. The distance r between the macrocycle and thread carbonyl groups can be obtained from the macrocycle–thread coupling β. The magnitude of this coupling is determined by both the angle and the distance between the coupled C=O groups in the macrocycle and thread (17). Because the angle is known from the cross-peak anisotropy, it is possible to obtain an estimate for the distance from the magnitude of the coupling, which can be done by using the dipole–dipole approximation for the coupling strength. In this approximation, which has been found to give a fairly accurate quantitative description of several different molecular systems (23, 41, 42, 44, 46), the coupling between two vibrational modes a and b is given by (41)

$$\beta = \frac{1}{4\pi\varepsilon_0}\left[\frac{\vec{\mu}_a\cdot\vec{\mu}_b}{r^3} - 3\frac{(\vec{r}\cdot\vec{\mu}_a)(\vec{r}\cdot\vec{\mu}_b)}{r^5}\right], \quad [3]$$

where $\vec{\mu}_i$ are the transition dipoles and $\vec{r}$ is the distance vector between the two transition dipoles. By applying this equation to the coupling β between proximate macrocycle and thread C=O-stretching modes, we can determine the distance r between these groups (see Fig. 1). The magnitudes of the transition dipoles can be obtained from the integrated absorption cross sections (47), and from the steady-state absorption spectrum we obtain $|\vec{\mu}_T| = 0.42$ debye (D) and $|\vec{\mu}_M| = 0.28$ D, where the indices refer to the thread and the macrocycle, respectively. Using a dipole–dipole angle of 48°, we find r = 6.9 ± 0.9 Å, which agrees reasonably well with the distance of 5.1 Å between the centers of the macrocycle and thread C=O groups in the crystal structure. The difference may be due to small differences between the crystalline and solution-phase coconformations. It could also be due to the dipole–dipole approximation, which overestimates the coupling at short distances (note that Eq. **3** diverges as r approaches zero). As a consequence, when using the dipole–dipole approximation, the estimate for the distance obtained from the coupling is slightly larger than the real value. A more accurate estimate of the distance can be obtained by using more sophisticated models for the vibrational coupling (48–50), and we hope the results presented here will stimulate work in this direction.

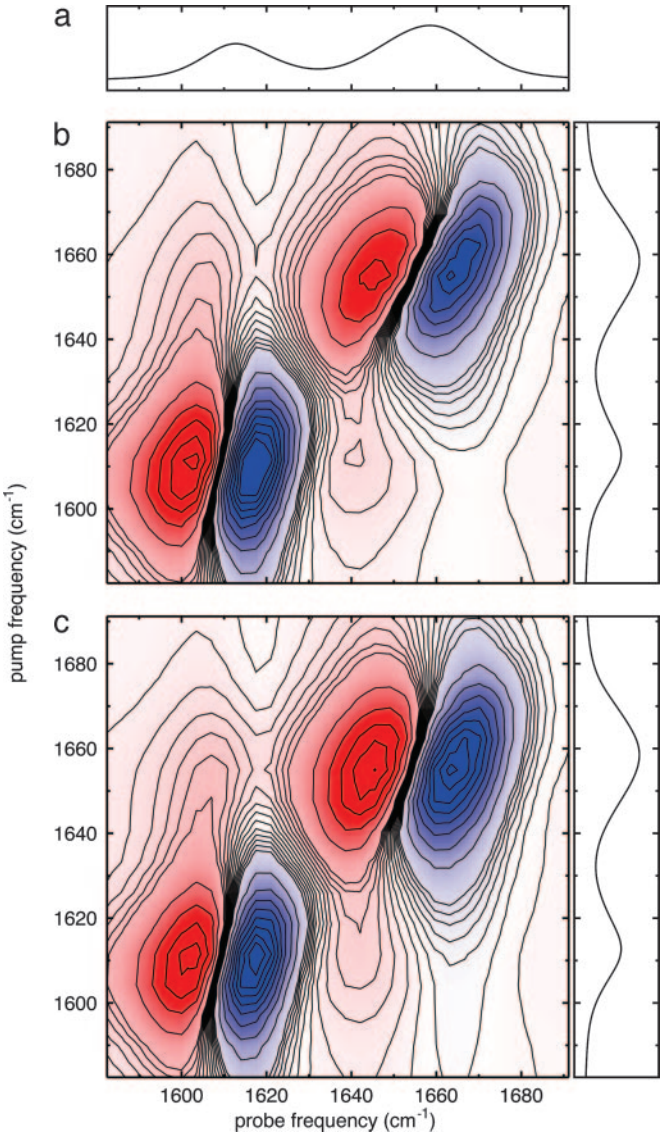

Fig. 4. Calculated 1D and 2D spectra obtained by using the couplings given in Eq. **1** and the best-fit values given in Table 1. (*a*) Calculated linear absorption spectrum. (*b*) Calculated 2D spectrum of the rotaxane at a pump-probe delay of 1 ps for parallel polarizations of the pump and probe pulses. Red indicates positive $\Delta\alpha$; blue indicates negative $\Delta\alpha$. The contour level spacing is the same as in Fig. 2*b*. (*c*) The same as in *b* but for perpendicular polarizations of the pump and probe pulses. The contour level spacing is the same as in Fig. 2*c*.

Semiquantitative Analysis. Interestingly, the macrocycle–thread angle θ can also be read off directly from the 2D-IR spectrum. If a cross-peak involves the coupling of two localized vibrations i and j, its anisotropy R_{ij} is directly related to the angle θ_{ij} between the transition-dipole moments of the two coupled modes: (17)

$$R_{ij} = \frac{3\cos^2\theta_{ij} - 1}{5}. \quad [4]$$

In the present case, the macrocycle and thread absorption bands are caused by more than one C=O group, and the situation is

slightly more complicated. However, because of the large inhomogeneities σ of the macrocycle and thread bands, a simplifying assumption can be made. The differences between the localized frequencies ε_3, ε_4, ε_5, and ε_6 of a rotaxane molecule are on the order of σ_M, which is much larger than the couplings between the C═O groups in the macrocycle (see Eq. **1**). As a consequence, the eigenstates of the macrocycle are localized on single C═O groups (17). The same argumentation holds for the thread. The cross-peaks can therefore be regarded to a good approximation as arising from the coupling between localized macrocycle and thread C═O-stretching modes, and the cross-peak anisotropy is related to the angle between the transition-dipole moments of these localized modes. Eq. **4** can then still be used to obtain a estimate of the angle θ between neighboring macrocycle and thread C═O groups, and from the observed anisotropy of -0.05, we obtain a value of $\approx 60°$ for θ, which agrees with the value obtained from the more detailed analysis above. This agreement shows that a simple analysis of the cross-peak anisotropy can be used to obtain structural information from the 2D-IR spectrum if the eigenstates are localized, as is often the case.

Conclusions

We have shown that 2D-IR spectroscopy can be used to determine the coconformation of a rotaxane with picosecond time resolution. In particular, the angle and distance between the carbonyl groups in the macrocycle and thread have been determined from the 2D-IR spectrum of the [2]rotaxane. It should be noted that the application of 2D-IR spectroscopy to molecular devices is by no means limited to devices containing carbonyl groups. In principle, the coupling between any pair of IR-active normal modes can be measured and used to determine the molecular structure.

Our results demonstrate the feasibility of time-resolved 2D-IR experiments in which externally triggered structural changes of molecular devices are measured with picosecond time resolution. In such experiments, the elementary mechanical motions of molecular devices can be observed in real time, making it possible to investigate the nature of these motions (inertial, diffusive, or hopping) and to determine which molecular degrees of freedom are involved. We believe that this approach will lead to insights into the functioning of molecular devices that are difficult to obtain through other experimental methods.

We thank Hinco Schoenmaker for technical support, Anouk Rijs and Dhiredj Jagesar for assistance during sample preparation, and Kobus Kuipers for critically reading the manuscript. This work was supported by the European Community (Exploiting Mechanical Motion of Molecular Architectures Research Training Network Contract HPRN-CT-2002-00168) and is part of the research program of the Stichting voor Fundamenteel Onderzoek der Materie, which is financially supported by the Nederlandse Organisatie voor Wetenschappelijk Onderzoek.

1. Sauvage, J.-P. & Dietrich-Bucheker, C., eds. (1999) *Molecular Catenanes, Rotaxanes, and Knots* (Wiley, Weinheim, Germany).
2. Balzani, V., Credi, A., Raymo, F. M. & Stoddart, J. F. (2000) *Angew. Chem. Int. Ed.* **39,** 3348–3391.
3. Balzani, V., Venturi, M. & Credi, A. (2003) *Molecular Devices and Machines: A Journey into the Nanoworld* (Wiley, Weinheim, Germany).
4. Kay, E. R. & Leigh, D. A. (2005) in *Functional Synthetic Receptors*, eds. Schrader, T. & Hamilton, A. D. (Wiley, Weinheim, Germany), pp. 333–406.
5. Brouwer, A. M., Frochot, C., Gatti, F. G., Leigh, D. A., Mottier, L., Paolucci, F., Roffia, S. & Wurpel, G. W. H. (2001) *Science* **291,** 2124–2128.
6. Altieri, A., Gatti, F. G., Kay, E. R., Leigh, D. A., Martel, D., Paolucci, F., Slawin, A. M. Z. & Wong, J. K. Y. (2003) *J. Am. Chem. Soc.* **125,** 8644–8654.
7. Flood, A. H., Stoddart, J. F., Steuerman, D. W. & Heath, J. R. (2004) *Science* **306,** 2055–2056.
8. Kelly, T. R., De Silva, H. & Silva, R. A. (1999) *Nature* **401,** 150–152.
9. Koumura, N., Zijlstra, R. W. J., vanDelden, R. A., Harada, N. & Feringa, B. L. (1999) *Nature* **401,** 152–155.
10. Leigh, D. A., Wong, J. K. Y., Dehez, F. & Zerbetto, F. (2003) *Nature* **424,** 174–179.
11. Hernandez, J. V., Kay, E. R. & Leigh, D. A. (2004) *Science* **306,** 1532–1537.
12. Kelly, T. R., Bowyer, M. C., Bhaskar, K. V., Bebbington, D., Garcia, A., Lang, F., Kim, M. H. & Jette, M. P. (1994) *J. Am. Chem. Soc.* **116,** 3657–3658.
13. Bedard, T. C. & Moore, J. S. (1995) *J. Am. Chem. Soc.* **117,** 10662–10671.
14. Badjić, J. D., Balzani, V., Credi, A., Silvi, S. & Stoddart, J. F. (2004) *Science* **303,** 1845–1849.
15. Kubo, R., Toda, M. & Hashitsume, N. (1985) *Statistical Physics II: Nonequilibrium Statistical Mechanics* (Springer, Berlin).
16. Ernst, R. R., Bodenhausen, G. & Wokaun, A. (1987) *Principles of Nuclear Magnetic Resonance in One and Two Dimensions* (Clarendon, Oxford).
17. Hamm, P., Lim, M., DeGrado, W. F. & Hochstrasser, R. M. (1999) *Proc. Natl. Acad. Sci. USA* **96,** 2036–2041.
18. Asplund, M. C., Zanni, M. T. & Hochstrasser, R. M. (2000) *Proc. Natl. Acad. Sci. USA* **97,** 8219–8224.
19. Woutersen, S. & Hamm, P. (2000) *J. Phys. Chem. B* **104,** 11316–11320.
20. Zanni, M. T., Ge, N. H., Kim, Y. S. & Hochstrasser, R. M. (2001) *Proc. Natl. Acad. Sci. USA* **98,** 11265–11270.
21. Golonzka, O., Khalil, M., Demirdöven, N. & Tokmakoff, A. (2001) *J. Chem. Phys.* **115,** 10814–10828.
22. Jonas, D. M. (2003) *Science* **300,** 1515–1517.
23. Demirdoven, N., Cheatum, C. M., Chung, H. S., Khalil, M., Knoester, J. & Tokmakoff, A. (2004) *J. Am. Chem. Soc.* **126,** 7981–7990.
24. Stolow, A. & Jonas, D. M. (2004) *Science* **305,** 1575–1577.
25. Bredenbeck, J., Helbing, J., Behrendt, R., Renner, C., Moroder, L., Wachtveitl, J. & Hamm, P. (2003) *J. Phys. Chem. B* **107,** 8654–8660.
26. Chung, H. S., Khalil, M., Smith, A. W., Ganim, Z. & Tokmakoff, A. (2005) *Proc. Natl. Acad. Sci. USA* **102,** 612–617.
27. Gatti, F. G., León, S., Wong, J. K. Y., Bottari, G., Altieri, A., Morales, M. A., Teat, S. J., Frochot, C., Leigh, D. A., Brouwer, A. M. & Zerbetto, F. (2003) *Proc. Natl. Acad. Sci. USA* **100,** 10–14.
28. Fyfe, M. C. T., Glink, P. T., Menzer, S., Stoddart, J. F., White, A. J. P. & Williams, D. J. (1997) *Angew. Chem. Int. Ed. Engl.* **36,** 2068–2070.
29. Sauvage, J.-P., ed. (2001) *Molecular Machines and Motors* (Springer, Berlin).
30. Bodis, P., Larsen, O. F. A. & Woutersen, S. (2005) *J. Phys. Chem. A* **109,** 5303–5306.
31. Mukamel, S. (1995) *Principles of Nonlinear Optical Spectroscopy* (Oxford Univ. Press, Oxford).
32. Tokmakoff, A. (2000) *J. Phys. Chem. A* **104,** 4247–4255.
33. Zanni, M. T., Asplund, M. C. & Hochstrasser, R. M. (2001) *J. Chem. Phys.* **114,** 4579–4590.
34. Demirdöven, N., Khalil, M. & Tokmakoff, A. (2002) *Phys. Rev. Lett.* **89,** 237401/1–237401/4.
35. Kwac, K. & Cho, M. (2003) *J. Chem. Phys.* **119,** 2256–2263.
36. Torii, H., Tatsumi, T. & Tasumi, M. (1997) *Mikrochim. Acta* **14,** 531–533.
37. Woutersen, S. & Hamm, P. (2001) *Chem. Phys.* **266,** 137–147.
38. Mukherjee, P., Krummel, A. T., Fulmer, E. C., Kass, I., Arkin, I. T. & Zanni, M. T. (2004) *J. Chem. Phys.* **120,** 10215–10224.
39. Volkov, V. & Hamm, P. (2004) *Biophys. J.* **87,** 4213–4225.
40. Kim, Y. S. & Hochstrasser, R. M. (2005) *J. Phys. Chem. B* **109,** 6884–6891.
41. Krimm, S. & Bandekar, J. (1986) *Adv. Protein Chem.* **38,** 181–364.
42. Hamm, P., Lim, M. & Hochstrasser, R. M. (1998) *J. Phys. Chem. B* **102,** 6123–6138.
43. Piryatinski, A., Tretiak, S., Chernyak, V. & Mukamel, S. (2000) *J. Raman Spectrosc.* **31,** 125–135.
44. Dijkstra, A. G. & Knoester, J. (2005) *J. Phys. Chem. B* **109,** 9787–9798.
45. Press, W. H., Teukolsky, S. A., Vetterling, W. T. & Flannery, B. P. (1992) *Numerical Recipes in C* (Cambridge Univ. Press, Cambridge, U.K.).
46. Krummel, A. T., Mukherjee, P. & Zanni, M. T. (2003) *J. Phys. Chem. B* **107,** 9165–9169.
47. Atkins, P. W. (1992) *Molecular Quantum Mechanics* (Oxford Univ. Press, Oxford).
48. Nafie, L. A. (1997) *Annu. Rev. Phys. Chem.* **48,** 357–386.
49. Choi, J. H., Cho, M. & Ham, S. Y. (2003) *J. Phys. Chem. B* **107,** 9132–9138.
50. Kubelka, J., Huang, R. & Keiderling, T. A. (2005) *J. Phys. Chem. B* **109,** 8231–8243.
51. Nitzan, A. & Jortner, J. (1973) *Mol. Phys.* **25,** 713–734.